3-9-2022

Influence of Cold Expansion and Aggressive Environment on Crack Growth in AA2024-T3

Ken Shishino
Embry-Riddle Aeronautical University

Christopher Leirer

Alberto Mello
melloa2@erau.edu

Influence of Cold Expansion and Aggressive Environment on Crack Growth in AA2024-T3

Ken Shishino,[1] Christopher T. Leirer[1], and Alberto W. Mello[2]
Embry-Riddle Aeronautical University, Daytona Beach, FL, 32114, USA

Published on March 2022. AIAA Journal. https://doi.org/10.2514/1.J061090

This research aims to establish the effect of hole cold expansion on fatigue life of pre-cracked material under aggressive environment. A relationship between crack propagation and secondary crack initiation was established for AA2024-T3 cold worked holes subjected to cyclic loads to determine the impact on fatigue life of joints in presence of saline solution. Galvanic corrosion of a steel fastener/aluminum plate assembly was investigated assuming the presence of cracks in the aluminum plates, whose growth will be monitored in-situ with a digital microscope throughout the fatigue process. The cold expansion treatment improved the fatigue life fourfold under a corrosive environment, and 11.3 times in a clean environment when compared to a plain hole. Corrosion revealed the possibility of a location shift in critical stress intensity factor, causing growth of the critical crack happening outside of the region where benefits of cold expansion can be achieved. The benefits of cold work expansion could be applied for pre-cracked materials for an improved inspection interval, but also calls for reevaluation of inspection area to prevent secondary crack initiation that could lead to ultimate failure of the structural component.

Nomenclature

b = outside radius

C = crack growth rate coefficient

c = crack length

c_p = plastic zone radius

[1] Graduate Student, Aerospace Engineering Department.
[2] Associate Professor, Aerospace Engineering Department, and AIAA Senior Member.

D_{in} = fastener hole diameter

D_m = mandrel diameter

E = Young's Modulus of Elasticity

K = stress intensity factor

K_c = plane stress fracture toughness

K_{calc} = "as-is" stress intensity factor

K_{cold} = stress intensity factor due to cold work expansion

K_{eff} = effective stress intensity factor

K_{i_c} = plane strain fracture toughness

K_{i_e} = effective fracture toughness

K_{max} = maximum stress intensity factor in a load cycle

K_{op} = opening stress intensity factor

M_f = free surface correction

NaCl = sodium chloride

n, p, q = empirical material constants

R = stress ratio

R_h = hole radius

r = distance from edge of hole

r_y = reverse yielding radius

t_s = sleeve thickness

wt.% = weight percent

ΔK = stress intensity factor range

ΔK_{th} = threshold stress intensity factor range

ν = Poison ratio

ρ = reverse yield radius

σ_a = amplitude stress

σ_m = average (mean) stress

σ_{max} = maximum stress

σ_{min} = minimum stress

$\sigma_{Ela.Rad.Res.}$ = circumferential stress in the radial direction (elastic region)

$\sigma_{Ela.Tan.Res.}$ = circumferential stress in the tangential direction (elastic region)

$\sigma_{Pla.Rad.Res.}$ = circumferential stress in the radial direction (plastic region)

$\sigma_{Pla.Tan.Res.}$ = circumferential stress in the tangential direction (plastic region)

$\sigma_{Rev.Rad.Res.}$ = circumferential stress in the radial direction (reverse yielding region)

$\sigma_{Rev.Tan.Res.}$ = circumferential stress in the tangential direction (reverse yielding region)

σ_x = local circumferential stress

τ_y = yield stress in pure shear

I. Introduction

One of the main cause of concerns that threatens the structural life of an aircraft is fatigue. Fatigue is the failure of a part or component after the repeated loading and unloading during use; oftentimes this cyclic loading that causes the failure is far lower than the known yield stress of the material that composes the part. Most frequently during the preparation and manufacturing stages of these structural components, the alloys undergo methods that improve the resistance to crack growth and fatigue endurance. While these methods use different mediums, the underlying purpose of the process is the same for them each.

The process investigated in this work is called hole cold expansion, which has become one of the most widely used hardening processes in the aerospace industry over the last 30 years [1]. This method typically involves forcefully expanding a pre-drilled fastener hole to a marginally wider diameter than the original drilling. During this expansion the material close to the edge of the hole is plastically deformed, at the same time the material at farther regions away from the edge of the hole only experience elastic deformation as the forceful expansion effect is lessened [2]. Once the expansion tool is removed from the fastener hole, the elastically surrounding areas have a strong reaction, forcing the permanently deformed region to return to the original starting configuration; this reaction creates a residual compressive stress region around the edge of the hole.

This residual compressive stress region tends to cancel part of the tensile stresses resulting from external loading thus reducing the stress concentration at the hole [3]. This residual stress region also inhibits the growth of and propagation of cracks through the specimen [4], thus improving the fatigue life. The expansion method used for this

research is the split-sleeve with mandrel, detailed in Fig. 1, which has become the most prominent method used in the aerospace industry [5, 6] because of advantages over the other types of expansion techniques. These advantages include good adaptability, high efficiency as multiple fastener holes can be expanded in quick succession, and the fact that it causes little damage to the surface of the hole. The split-sleeve method also requires access to one side of the component only, which is very appealing during the assembling phase.

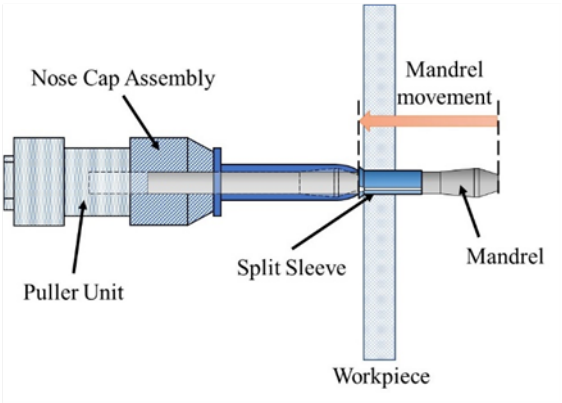

Fig. 1 Schematic diagram of the split-sleeve tapered mandrel assembly that will be used as the cold expansion method for this research.

II. Literature Review

Investigations into fatigue and the technology that can be used to overcome the negative effects that result from fatigue have gone on for more than 60 years in the aerospace industry. Academic researchers and industrial companies, such as The Boeing Company, and professionals alike have been looking at ways to counteract and even prevent fatigue crack growth. One of the earliest and most prominent research into the effects of cold expansion was performed by Phillips in 1974. In this study, Phillips conducted an investigation on different parameters to optimize the expansion process with the split-sleeve method [7]. In 2003, Chakherlou and Vogwell examined the effects that mandrel only cold expansion had on the fatigue life of specimens undergoing sinusoidal constant amplitude loading and stress ratio, R, of zero [8]. Also in 2003, Zhang and Wang examined the improvements in fatigue life that cold expansion has when applied to specimens that have already undergone some level of fatigue as opposed to application at the manufacturing stage [9]. Liu et al. investigated the development of the residual stress region around the fastener hole during the expansion process in 2008. They also examined the effect that different degrees of expansion, ranging from 2% to 6%, had on the fatigue life of specimens while undergoing constant amplitude sinusoidal loading at a stress ratio of 0.1 [3]. In 2010, Gopalakrishna et al. examined the effect that two different split-sleeve methods, tapered mandrel and

ball techniques, had on the fatigue performance of AA2024-T3 expanded holes with varying levels of expansion degrees, 1 to 6 percent [5]. Most recently in 2017, Wang et al. investigated the fatigue performance of cold expanded holes of 6061-T6 Aluminum alloys to explore the benefits gained by expansion when compared to as-drilled specimens [2].

Another popular topic of investigation regarding structural life of an aircraft is corrosion, as it is one of the common failure modes seen in aircraft components. A report from the U.S. Air Force has revealed that "more than 80% of structural failures of aircrafts originated from corrosion pits" [10]. While issues with corrosion are a clear threat to safety, it also holds economic significance. Czaban points out that the direct annual cost associated with corrosion in the United States aerospace industry in 2002 has been estimated to be $2.2 billion, including costs for maintenance, downtime, and manufacturing [11]. The topic of corrosion in the aerospace industry can also be a complex issue, because aircraft structures, for its purposes, transport through various "geographical location, aircraft range, local climate and changes in weather" which can vary the initiation of corrosion [11].

In this research, galvanic corrosion is mainly featured as corrosion on aircraft structures often occurring at joints where dissimilar metal materials may come in contact. Galvanic corrosion is a type of corrosion induced when two dissimilar materials are coupled in a corrosive electrolyte [12]. In 2018, Nicolas et al. examined the relationship of mechanical deformation and localized corrosion at the mesoscale level for a 316L stainless steel fastener and AA7050-T7451 assembly [13]. In 2019, Nicolas et al. proceeded to further investigate the relationship of mechanical deformation and localized corrosion for an actively loaded structural component [14]. These studies showed significance in characterizing the effect of mechanical and chemical mechanisms in terms of corrosion of a material under constant loading.

While reviewing previous researches which examine the various aspects of cold expansion and galvanic corrosion, there is still one question not answered: what is the impact on the fatigue life the cold expansion has when applied to fastener holes already containing micro or small cracks, and also, in presence of corrosive environment? This research builds on that of Zang and Wang in 2003, where their specimens were fatigued some percentage of their lives but there was not necessarily a crack present at the time of expansion [9]. For this research, the formation of a through crack at the fastener hole is confirmed at the time of application of the expansion. The goal of this research was to examine if there is in fact any noticeable improvements in the fatigue life of AA2024-T3 specimens that have a small

crack present at the fastener hole. Furthermore, specimens were subjected to aggressive environment to simulate applications such as naval aircrafts.

III. Methodology

The process of this research can be broken down into two distinct stages: preparation and experimentation. The preparation stage involved dimensioning and manufacturing of the specimens and the experimentation involved fatigue testing, cold expansion treatment, and corrosion of the specimen. In this section, the material selection, equipment, and procedures of both preparation and experimentation are discussed.

A. Specimen Material

The importance of having a material that provides high strength while also maintaining relatively low weight has led to a majority of aircraft structures to be primarily composed of aluminum alloys [15], with the most widely used alloy being AA2024-T3. AA2024-T3 is typically chosen for applications that require high strength-to-weight ratio and also good fatigue resistance [16]. Because of these requirements, AA2024-T3 was chosen for the purpose of this experiment. The basic material properties for an AA2024-T3 alloy sheet of thickness 3.18 mm are provided in Table 1 [17]. It is to be noted that the material properties were found for the thickness of the specimen used in the experimentation, which will be discussed later in this section.

Table 1 Material properties of AA2024-T3 alloy used for experimentation [17].

Property	Value	
Young' Modulus, E	72.4 GPa	(10.5×10^3 ksi)
Plasticity Modulus	0.607 GPa	(88.0 ksi)
Yield Strength	324 MPa	(47.0 ksi)
Ultimate Strength	441 MPa	(64.0 ksi)
Poison ratio, ν	0.33	(0.33)
Density	2.78 g/cm^3	(0.10 lb/in^3)

B. Dimensioning and Manufacturing of Experimental Specimens

Dimensioning of experimental specimens was a vital step in the overall process of the research. Using Elastic-Plastic Theory, appropriate dimensions were determined to ensure that the benefits of cold expansion were not inhibited. Essentially, if the specimen width is too narrow, the edge distance may not be enough to create sufficient spring back reaction to form a significant residual stress region. This limitation could lead to a degradation in the performance of the stress region and reduce the benefits created. Therefore, a prediction of the actual stress distribution

was considered in sizing the specimen. In addition, the authors have followed the good practices in the aviation industry to consider an edge distance equal to at least three times the radius of the fastener hole. The length of the specimen also required the need for adequate material for gripping to be taken into consideration. If there was too little material lengthwise the material could not be gripped by the tensile machines adequately, nor would there be enough material for the applied stresses to be homogenized in the gauge section.

Dimensioning of the fastener hole size was dependent on two factors. The first factor was that the desired cold expansion percentage be within the accepted industry range. Equation 1 shows the calculation of the expansion percentage depends on three parameters: the mandrel diameter, sleeve thickness, and fastener hole diameter. Only the hole diameter was able to be manipulated as we have previously fixed the mandrel diameter and split-sleeve thickness.

$$CE\% = \frac{(D_m + 2t_s) - D_{in}}{D_{in}} \cdot 100\% \quad (1)$$

Where D_m is the mandrel diameter, t_s is the sleeve thickness, and D_{in} is the fastener hole diameter. The second factor that led to the fastener hole diameter sizing is the ability to conform to traditional drill bit sizing. There are common drill bit sizes that are readily available and found in industry, so conforming to sizes similar to these was decided. It is also worth noting that the thickness of experimental specimens was determined by the thickness of the AA2024-T3 sheet. Engineering drawings of the specimen were created and provided to the Embry-Riddle Aeronautical University Manufacturing Shop for production. An example of the dimensioned engineering drawings provided to the manufacturing shop and a fabricated AA2024-T3 specimen can be seen in Fig. 2 and Fig. 3 respectively.

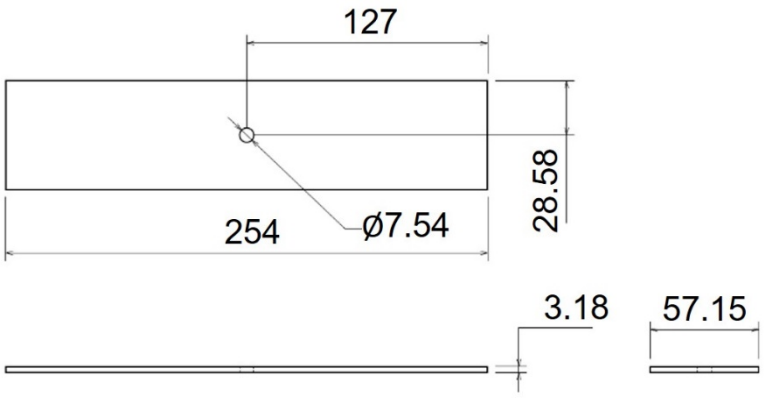

Fig. 2 Engineering drawings of AA2024-T3 specimen with dimensions in mm.

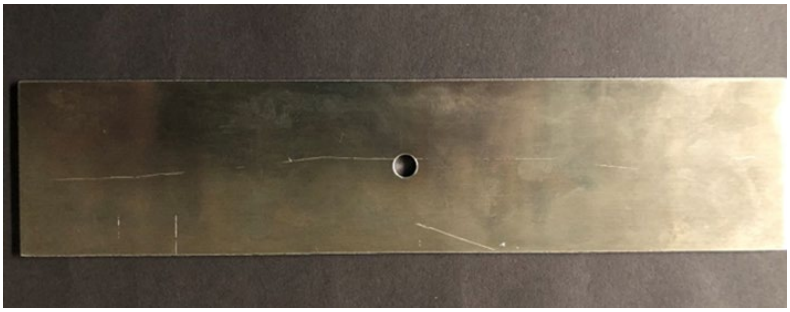

Fig. 3 Fabricated AA2024-T3 experimental specimen.

The specimen was then taken to a Buehler Ltd. Twin Variable Speed Grinder-Polisher machine to remove any surface scratch that may lead to undesired crack initiation on the specimen. A 600-grit sandpaper by LECO Corporation was first used to wet sand the area of interest followed by a MicroCloth polishing cloth from Buehler Ltd. with 5μ de-agglomerated alpha alumina solution, also by LECO Corporation, to remove any small remaining scratches. Then, after replacing the polishing cloth with a new MicroCloth, a solution of 1μ de-agglomerated alpha alumina was used to further polish the sample until surface scratches were not visible. Fig. 4 shows the equipment used in the polishing procedures for the specimens. For the fatigue under corrosion experiments, a latex sleeve was fixed to the specimen for holding the saline solution-soaked sponge at the fastener hole. The specific material was chosen for its waterproof characteristic as well as its elastic characteristic for ease of observation during the experiment. Fig. 5 shows the final product used in the experimentation.

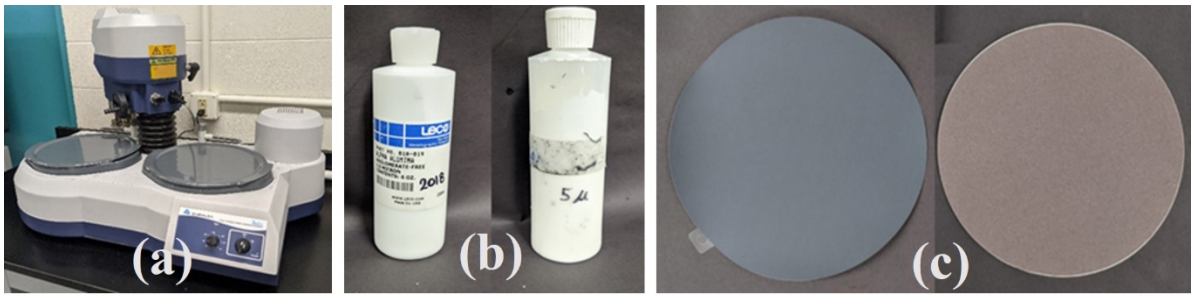

Fig. 4 Equipment for specimen polishing (a) Twin Variable Speed Grinder-Polisher (b) agglomerate-free alpha alumina solutions (c) sandpaper and polishing cloth.

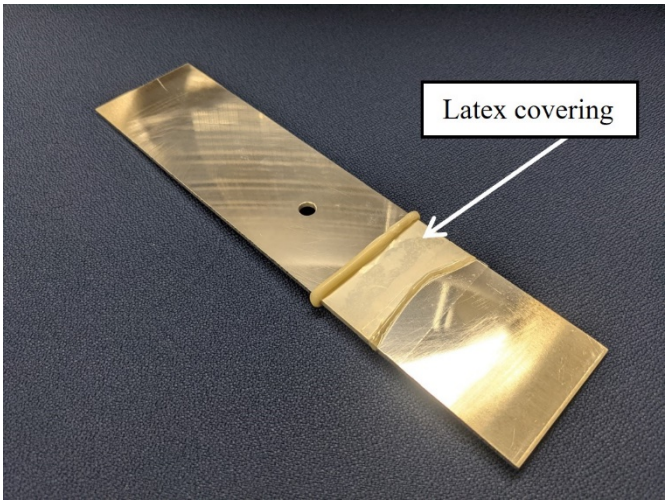

Fig. 5 Prepared AA2024-T3 experimental specimen for fatigue under corrosion.

C. Fatigue Testing of Experimental Specimens

Crack Initiation Process

In this research, an application with a pre-cracked condition is assumed. In order to meet this requirement, an initial flaw was induced in the sample. A small cut was applied at the inner wall of the hole, perpendicular to the loading direction, using a thin razor blade. The cut is shown in Fig. 6. By applying this cut, the starting point of the crack initiation could be controlled for observation as well.

The specimen was then fixed onto a fatigue testing setup, MTS Model 204.61 Hydraulic Piston Actuator, MTS 661.21A-02 Load Cell, and a pair of MTS Series 647 Hydraulic Wedge Grips to apply cyclic tensile loads on the specimen. A UHM350-11 digital HDMI microscope was placed in front of the hole to capture images for observation and measurement of the crack growth by utilizing the Kopa Capture Software. The full configuration of the setup is shown in Fig. 7.

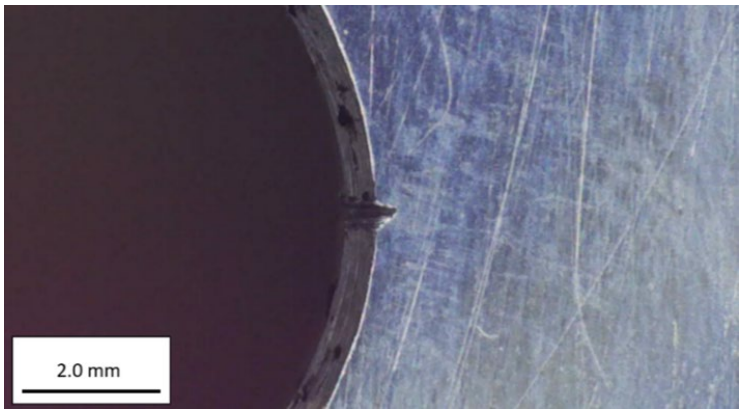

Fig. 6 Example of initial flaw induced on inner hole surface.

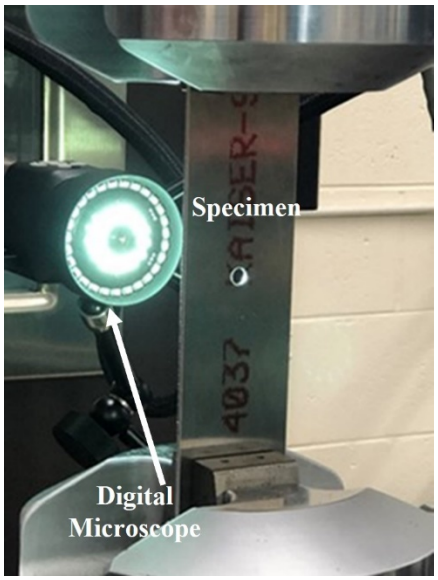

Fig. 7 Setup of specimen on fatigue testing machine.

The testing machine was set to apply an amplitude load of 16.01 kN and a mean load of 19.57 kN, inducing stresses tabulated in Table 2. The amplitude stress, σ_a, is determined by the range between the maximum and minimum stresses applied during the cycles. While σ_m is the mean point between the maximum and minimum stress values, where the maximum and minimum stress values are symbolized by σ_{max} and σ_{min} respectively. R is the ratio between the minimum and maximum applied stresses. This fatigue control variables are represented in Eqs. 2 through 4 below.

$$\sigma_a = \frac{\sigma_{max} - \sigma_{min}}{2} \tag{2}$$

$$\sigma_m = \frac{\sigma_{max} + \sigma_{min}}{2} \tag{3}$$

$$R = \frac{\sigma_{min}}{\sigma_{max}} \tag{4}$$

Table 2 Cyclic stress parameters for fatigue testing.

Variable	Value	
σ_a	88.25 MPa	(12.8 ksi)
σ_m	107.9 MPa	(15.64 ksi)
R	0.1	(0.1)

Another important factor of fatigue testing is frequency, which represents the number of cycles the component experiences in a period of time. The frequency of the cyclic loads was set to 1 Hz. The loads and frequency were designed to apply a continuous wide range of low to high tensile loadings while being slow enough to monitor crack initiation. The machine was stopped at every 250 cycles to check for crack initiation. Using the various lighting settings on the digital microscope and the digital zoom feature on the Kopa Capture Software, images with the best representation of the crack were taken. The images were then compared in attempt to find the slightest sign of crack initiation from the small cut. This procedure was repeated until crack initiation could be observed. The controlled experiment would proceed to the crack propagation phase, while other specimens are treated with cold expansion as discussed in the following section.

Cold Work Hole Expansion Process

Once it was determined that a crack had initiated, cold work expansion was applied on the hole similarly seen in the Fig. 1 diagram. The equipment used was the mandrel, the hand puller, and a split sleeve, as well as a set of wrenches including a size 3.175 cm socket wrench and 1.11 cm wrench as shown in Fig. 8. The hand puller was used in combination with the wrenches to manually pull the lubricated mandrel with split-sleeve through the specimen hole. It is important to note that the split in the sleeve was facing in the loading direction of the specimen as seen in Fig. 9. Excess grease was wiped from the specimen and hole surface to obtain a clear image of the crack using the digital microscope. Similarly to the crack initiation procedure, various lighting settings and the digital zoom were utilized for the best representation of the crack. During the crack propagation process, the current image was always compared with the reference image, taken at zero cycle.

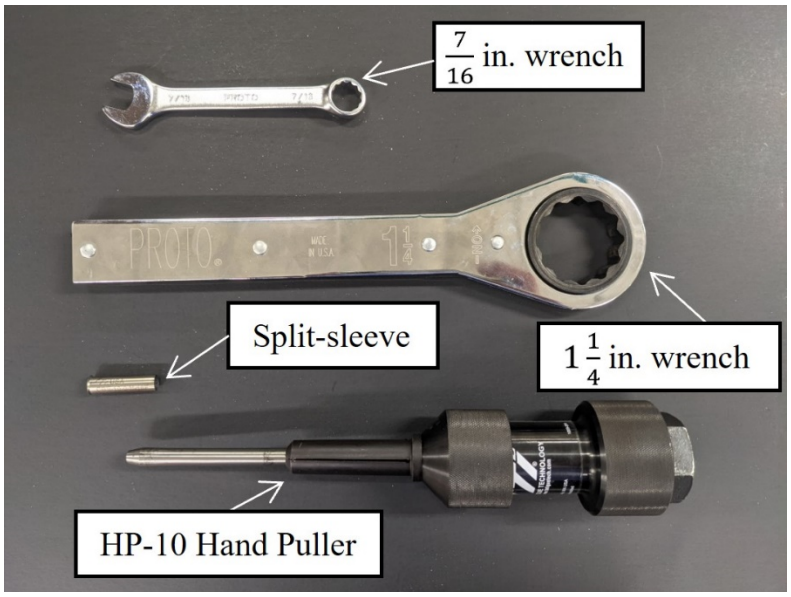

Fig. 8 Equipment for cold expansion process.

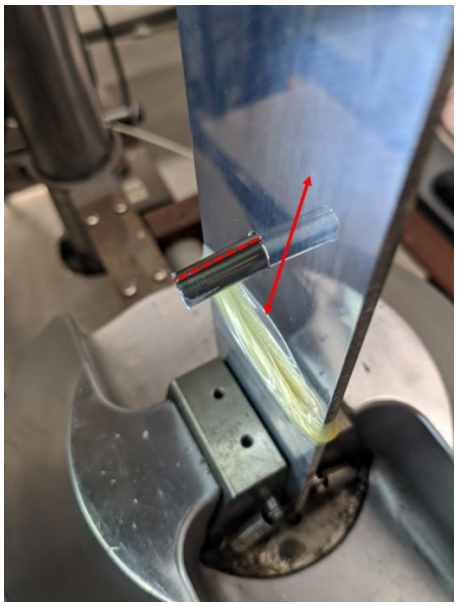

Fig. 9 Split-sleeve direction.

Crack Propagation Process

Experiments were conducted to, first, establish a reference fatigue life of a controlled specimen of a pre-cracked hole without cold expansion treatment. Then, the following experiments were designed to examine the benefits of cold expansion treatment on the pre-cracked hole. Examination was then extended to observe the effects of this

treatment for applications in an aggressive environment. In this section, the crack propagation process of the three conditions will be discussed.

Once the expansion treatment was provided to the pre-cracked hole, the crack propagation process between the control and treated specimens was the same. This propagation involved the application of cyclic loading, as described in Table 2, until the ultimate failure of each specimen. During the propagation process, each specimen underwent at maximum 1,000 cycles at a time to ensure that the growth of the crack could be tracked during the process. At the end of each set of cyclic periods, the crack would be opened and an image would be taken with the digital microscope to capture the crack length at its present size. The crack opening was created by inputting the maximum value of the cyclic stress, 196.15 MPa, into the MTS 407 Controller that was used to control the fatigue cycles. Having the specimen under tension allows for easy visualization of the crack as well as to accurately determine the crack tip position. The length of the crack from the edge of the fastener hole to the tip of the crack was determined by using these images and the calibrated measuring tools of the Kopa Capture Software. It should be noted that the measured crack lengths are the distance of the crack tip starting at the edge of the fastener hole, not the sole distance of the propagation path. The number of cycles per observation was modified as the crack growth rate increased to ensure proper capture of the propagation.

Additional procedures were added for conducting experimentation under aggressive environment. An AISI316 stainless steel bolt and nut of 6.35 mm (0.25 in.) diameter and 19.05 mm (0.75 in.) in length were attached at the hole after cold work expansion was applied. The bolt and nut were applied just enough for the surface of the steel to be in contact with the aluminum specimen, so that galvanic corrosion could be introduced without creating a stress concentration due to excessive tightening from the bolt and nut. Next, a layer of sponge was applied on both sides of the bolt and nut. The latex covering was raised up to the upper edge of the sponge, then the saline solution (3.5 wt.% NaCl solution) was slowly soaked into the sponge from the top. The solution was produced by combining appropriate amounts of distilled water and commercially available plain table salt to obtain for the desired weight percentages. Fig. 10 illustrates the equipment and materials for inducing the galvanic corrosion.

During this process, signs of leakage from the latex covering were checked, as this could potentially corrode the metal grips on the fatigue testing machine, shown in Fig. 11, as well as cause the specimen to slip from the grips. As an additional precaution, a paper towel or sponge was attached at the bottom end of the latex covering to absorb any small leakages.

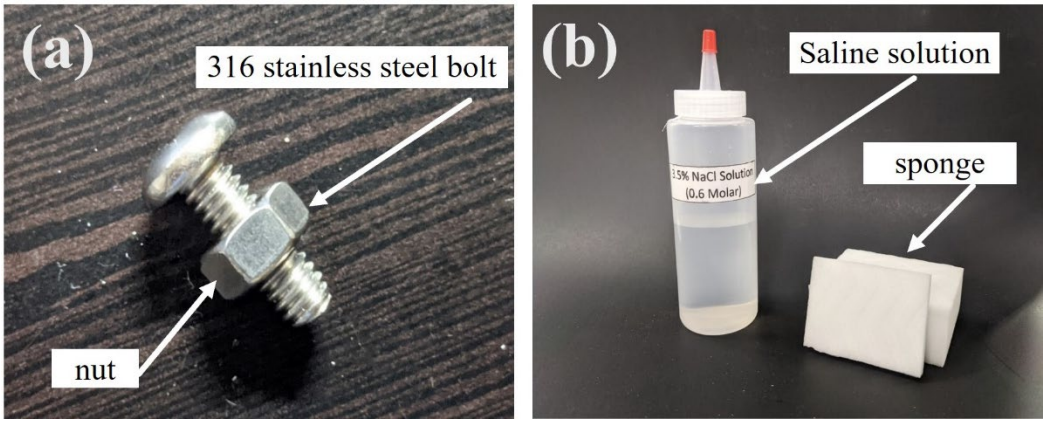

Fig. 10 (a) 316 stainless steel bolt and nut (b) 3.5 wt.% NaCl solution and sponge.

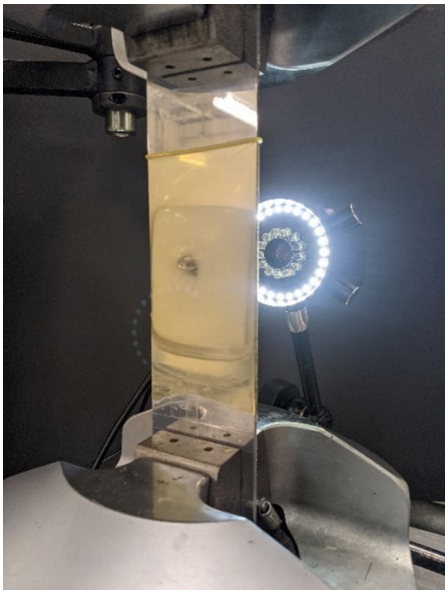

Fig. 11 Specimen setup under corrosive environment.

The specimen was then subjected to cyclic stresses as described in Table 2, until the ultimate failure of each specimen. The growth of the crack propagation caused by the corrosive environment was set to be observed every 24 hours. The increments of the number of load cycles were adjusted accordingly based on how quickly the crack grew. Similarly, the frequency setting on the fatigue testing machine was calculated based on the target number of cycles to be completed during the 24-hour time slot. Because fatigue under aggressive environment is sensitive to frequency, a frequency that would give the entire experiment a window between 5-10 days and be coherent with corrosion evolution along intermetallic particles in the alloy with formation of pitting according to Nicolas et al. [13, 14] was chosen.

After each set of load cycles were completed, the latex sleeve was lowered, and the sponges were taken out. Then, the bolt and nut were detached and the moisture on the specimen surface was gently removed with a paper towel. The

digital microscope was utilized to take images of the crack growth. A rubber-like material, such as an eraser, was used to carefully remove oxides and salt concentration from the specimen surface to obtain a clearer image of the crack tip.

A total of three specimens subjected to corrosion were tested. The objective of the first experiment was to observe the crack growth rate and the number of cycles that the specimen could take under corrosive environment. The duration of this experiment was set at seven days to obtain sufficient results in order to better predict and adjust increments of the observations and set appropriate durations for the experiment. The second experiment was set for ten days in hopes for observations in smaller increments once the crack growth rate significantly increases toward the end of its fatigue life. Finally, the third experimentation was designed to further validate a hypothesis built based on the results from the second corrosion experimentation.

IV. Results

A. Analytical Calculations for Cold Expansion

As mentioned in the previous section, the dimensioning of the specimen came from the result of iteratively using Elastic-Plastic Theory Equations to determine the system external diameter and hole diameter that would allow for adequate radial and tangential residual compressive stresses within the specimen external boundary. With this iterative calculation combined with the pre-defined mandrel diameter and split-sleeve thickness, the cold expansion percentage to be applied to the fastener hole was found to be 4.95%. This value is appropriate because it was desired to have a cold expansion degree similar to what is conducted in the industry, which is between 4 and 5 percent. Other important values that were found through analytical calculations can be found in Table 3.

Table 3 Important values from equations of Elastic-Plastic Theory.

Measurement	Value
Cold Expansion %	4.95%
Radial Displacement	0.189 mm
Plastic Zone Radius, c_p	13.7 mm
Reverse Yielding Radius, r_y	4.468 mm

There are three main regions that appear around a cold worked hole. Those are the plastic region, the reverse yielding region, and the elastic region. The reverse yielding radius is defined as the point with the maximum value of compressive tangential stress, which can be visualized at the position of 0.698 mm from the border of the hole in Fig. 12, corresponding to a distance (measured from the center of the hole) of 4.468 mm. Equations 5 and 6, which are

taken from studies by Cardinal et al. [18] and the manual associated with the Crack 2000 Damage Tolerance analysis tool [19], are circumferential stresses at the radius of the point of interest, *r*, in the plastic region. Equation 5 depicts the residual stress in the radial direction whereas Eq. 6 is in the tangential direction. Variables used in these equations include τ_y, the yield stress in pure shear, c_p, plastic zone radius, b, outside radius, and ρ, reverse yield radius.

$$\sigma_{Pla.\,Rad.\,Res.}(r) = -\tau_y\left[1 - \frac{c_p^2}{b^2} + ln\left(\frac{c_p^2}{r^2}\right)\right] + 2\tau_y\left[1 - \frac{\rho^2}{b^2} + ln\left(\frac{\rho^2}{r^2}\right)\right] \tag{5}$$

$$\sigma_{Pla.\,Tan.\,Res.}(r) = \tau_y\left[1 + \frac{c_p^2}{b^2} - ln\left(\frac{c_p^2}{r^2}\right)\right] - 2\tau_y\left[1 + \frac{\rho^2}{b^2} - ln\left(\frac{\rho^2}{r^2}\right)\right] \tag{6}$$

Similarly, equations for the residual stresses exist for the other two regions as shown in the following equations presented by Mello [19]. Equations 7 and 8 depict the circumferential stresses in the reverse yielding region, and Eq. 9 and 10 represent the circumferential stresses in the elastic region.

$$\sigma_{Rev.\,Rad.\,Res.}(r) = -\tau_y\left[1 - \frac{c_p^2}{b^2} + ln\left(\frac{c_p^2}{r^2}\right)\right] + 2\tau_y\frac{\rho^2}{b^2}\left[\frac{b^2}{r^2} - 1\right] \tag{7}$$

$$\sigma_{Rev.\,Tan.\,Res.}(r) = \tau_y\left[1 + \frac{c_p^2}{b^2} - ln\left(\frac{c_p^2}{r^2}\right)\right] - 2\tau_y\frac{\rho^2}{b^2}\left[\frac{b^2}{r^2} + 1\right] \tag{8}$$

$$\sigma_{Ela.\,Rad.\,Res.}(r) = -\tau_y\frac{c_p^2}{b^2}\left(\frac{b^2}{r^2} - 1\right) + 2\tau_y\frac{\rho^2}{b^2}\left[\frac{b^2}{r^2} - 1\right] \tag{9}$$

$$\sigma_{Ela\,Tan.\,Res.}(r) = \tau_y\frac{c_p^2}{b^2}\left(\frac{b^2}{r^2} + 1\right) - 2\tau_y\frac{\rho^2}{b^2}\left[\frac{b^2}{r^2} + 1\right] \tag{10}$$

Using the values in Table 3 combined with the Elastic-Plastic Equations shown above yielded the graph shown in Fig. 12, which shows the development of the residual radial and tangential stresses calculated from the edge of the hole.

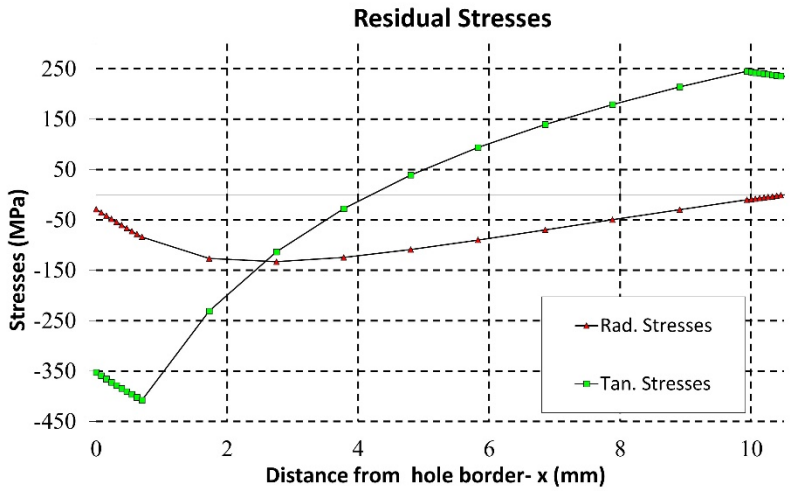

Fig. 12 Tangential and radial residual stress region development from the hole edge.

It can be seen in Fig. 12, the tangential residual stress region is the most important aspect of the residual stress because it is the most compressive near the edge of the hole, and it acts perpendicularly to the expected crack front. This tangential stress features reasonable compression in a range of up to 4.0 mm away from the hole edge. The rational is that this compression leads to the improvement in fatigue life as it must be overcome for crack propagation. The radial residual stress region development shows the importance of factoring in the Elastic-Plastic Theory Equations when it came to the dimensioning of the specimens. As it can be seen, the region does not zero out until more than 10.0 mm away from the hole edge, necessitating the adequate dimensioning to avoid compromising the residual stress development. For the specimen, the distance from the hole edge to the specimen border was determined to be 24.8 mm, what guarantees the proper stress distribution over the crack propagation region.

B. Numerical calculation cold expansion

With the purpose to confirm the residual stress field around the hole, we have performed a 3-D nonlinear static FEM for the cold work with the proposed expansion using FEMAP v11.4.2 with NX Nastran solver. In this case, we simulated the mandrel being fully pulled through the hole. The material properties of Al 2024-T3 were input into the respective section, both linear and nonlinear properties. The stress-strain points were found from mapping the stress-strain curve presented by Rice et al. [20]. In order to simulate the cold expansion process, a ramp function was generated that applied a surface pressure up to a maximum value following a linear trend over the period of 0.5 s and then decreased the surface pressure back to a zero value by the end of the 1.0 s. The maximum value with this generated function is meant to correspond to the point in the cold expansion process when the thickest part of the mandrel is

inside the fastener hole, providing the expansion, and the minimum value corresponds to the mandrel being removed from the fastener hole. Figure 13 depicts the applied function, being the factor the value multiplied by the maximum expansion.

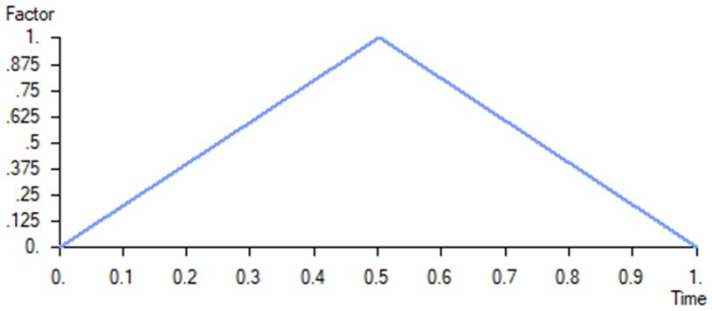

Fig. 13 Ramp function generated in FEMAP to modify the surface pressure applied as a function of time.

Figure 14 shows the evolution of the von Mises stress as cold work is applied in the FEM simulation. Figure 14(a) depicts the stress map when the mandrel is fully inserted in the hole (0.5 s), and the von Mises stress reaches a maximum value of 345 MPa, exceeding the yield stress of the material, starting the process of hardening in the affected area, as predicted. The analysis also shows that the stress goes down to reduced value about 10 mm from the hole border, confirming the safety of the chosen dimensions for the cold expansion experiments. Figure 14(b) displays the residual stress as predicted by the simulation, in terms of equivalent tensile stress. In this case, the simulation predicts the residual stress will extend to near 3 mm from the edge of the hole, what is below what was calculated by the analytical method. Despite the difference, both methods confirm the creation of compressive stress zone and the safety for the level of cold expansion in the specimen with the designed dimensions.

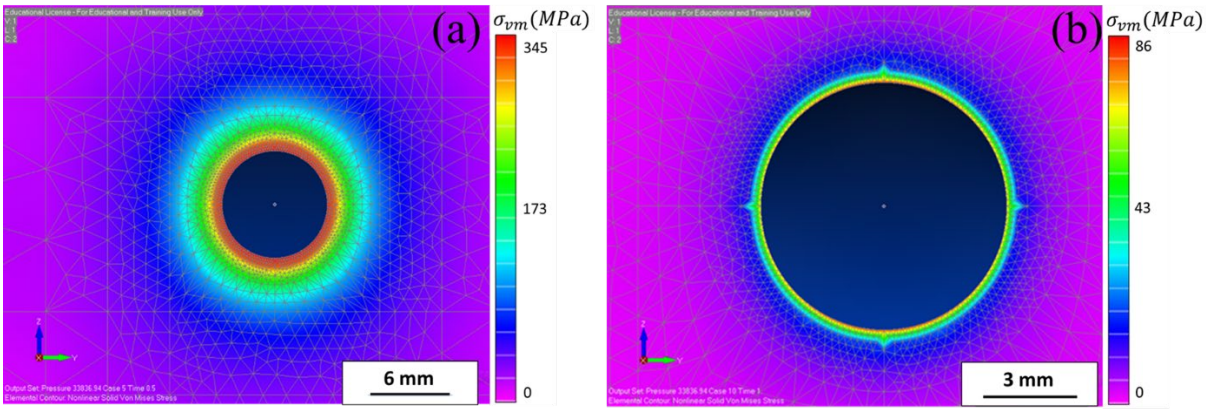

Fig. 14 Von Mises stress developed around the hole during the cold expansion process at (a) 0.5 s (mandrel fully inserted), and (b) 1.0 s (mandrel fully removed – residual stress).

C. Fatigue Testing

Fatigue Testing in Laboratory Environment

The as-drilled specimen which did not experience any treatment or aggressive environment was fatigued to failure using the methods as mentioned above. This specimen was able to sustain 6,256 cycles from the 0.254 mm initial crack, when undergoing the prescribed loading parameters. Table 4 highlights the crack length measurements that were taken at the end of each cycle period and would be used for comparison plotting later on. It can be seen though from Table 4, how fast the crack grew from the very onset of the fatigue loading. Images taken of the crack growth during this trial can be seen in Fig. 15 with the tip of the crack being highlighted in each image. Interestingly in this experiment, the crack initiated above the centerline of the hole, in a more favorable induced flaw. This caused the crack to propagate through a biaxial state of stress, following the most favorable path in a combination of grain arrangements and/or local state of stress. As the crack gets away from the influence of the hole, the crack slowly returns to a horizontal propagation perpendicularly to the applied load.

Table 4 Cycle count and crack length for as-drilled specimen.

Cycle Number	Crack Length (mm)	Cycle Number	Crack Length (mm)
0	0.254	**3,800**	3.531
800	0.813	**4,800**	5.359
1,800	1.524	**5,800**	8.585
2,800	2.337	**6,256**	10.73

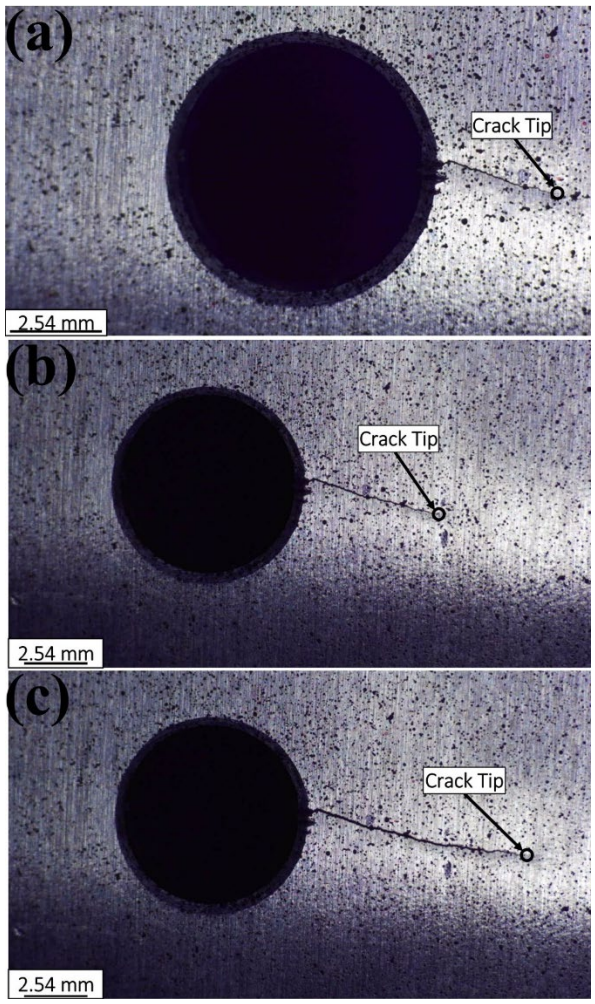

Fig. 15 Crack growth for as-drilled specimen during fatigue testing with crack tip location noted (a) 3,800 cycles (b) 4,800 cycles (c) 5,800 cycles.

The second fatigue test was conducted after the specimen had undergone the 4.95% expansion treatment but was not in the aggressive environment. This test was conducted to examine the effect that expansion would have when applied to pre-cracked components. The 4.95% CE Specimen had an extended fatigue life as compared to the control specimen, with a final cycle count of 70,983. This time to failure was 11.3 times greater than that of the control specimen and the rate of the crack growth can be seen in Table 5 below. Here, one can see the minute changes in the crack length during a large portion of the fatigue life of the specimen. Images of crack growth taken during the fatigue experiment of the 4.95% CE specimen can be seen in Fig. 16 and highlight the minimal crack growth shown in Table 5.

Table 5 Cycle count and crack length for the cold expanded hole.

Cycle Number	Crack Length (mm)	Cycle Number	Crack Length (mm)	Cycle Number	Crack Length (mm)	Cycle Number	Crack Length (mm)
0	0.254	**14,000**	0.965	**31,500**	1.194	**52,500**	1.702
500	0.305	**15,000**	0.991	**32,500**	1.194	**53,500**	1.702
1,000	0.356	**16,000**	0.991	**33,500**	1.219	**54,500**	1.727
1,500	0.406	**17,000**	1.016	**34,500**	1.219	**55,500**	1.778
2,000	0.406	**18,000**	1.016	**35,500**	1.219	**56,500**	1.829
2,500	0.432	**19,000**	1.016	**36,500**	1.219	**57,500**	2.057
3,000	0.432	**20,000**	1.041	**37,500**	1.245	**58,500**	2.108
3,500	0.457	**21,000**	1.067	**38,500**	1.295	**59,500**	2.235
4,000	0.508	**21,500**	1.092	**39,500**	1.295	**60,500**	2.311
4,500	0.533	**22,000**	1.092	**40,500**	1.346	**61,500**	2.616
5,000	0.584	**22,500**	1.118	**41,500**	1.448	**62,500**	2.896
5,500	0.610	**23,000**	1.143	**42,500**	1.448	**63,500**	3.226
6,000	0.610	**23,500**	1.143	**43,500**	1.473	**64,500**	3.607
6,500	0.610	**24,000**	1.168	**44,500**	1.499	**65,500**	4.013
7,000	0.610	**24,500**	1.168	**45,500**	1.676	**66,500**	4.572
8,000	0.660	**25,500**	1.194	**46,500**	1.676	**67,500**	5.232
9,000	0.686	**26,500**	1.194	**47,500**	1.676	**68,500**	5.994
10,000	0.711	**27,500**	1.194	**48,500**	1.676	**69,500**	6.782
11,000	0.762	**28,500**	1.194	**49,500**	1.676	**70,500**	8.687
12,000	0.889	**29,500**	1.194	**50,500**	1.676	**70,983**	9.533
13,000	0.889	**30,500**	1.194	**51,500**	1.676		

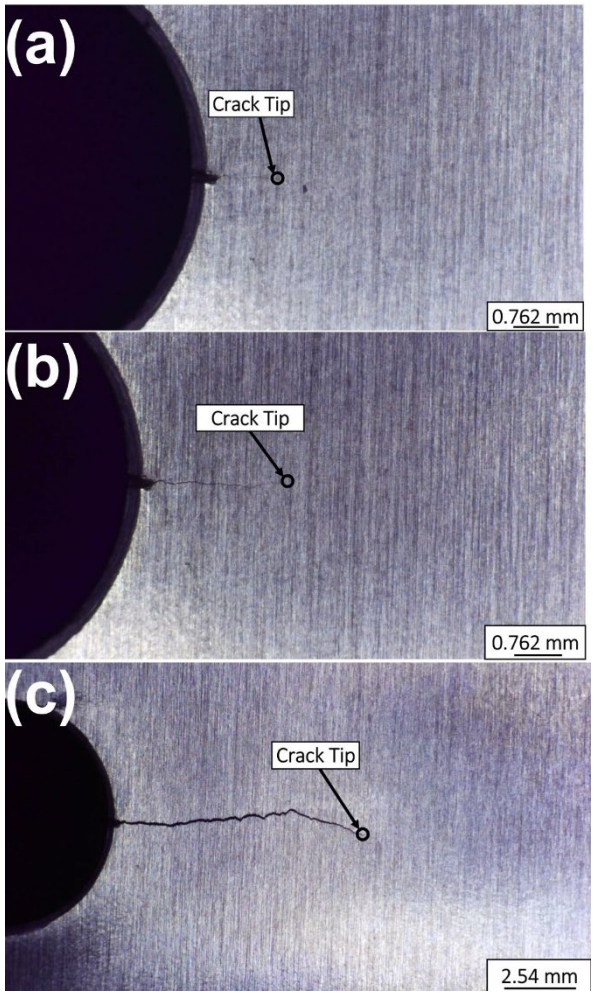

Fig. 16 Crack growth for 4.95% CE specimen during fatigue testing with crack tip location noted (a) 30,500 cycles (b) 60,500 cycles (c) 70,500 cycles.

A comparison of the fatigue life for both specimens can be seen in Fig. 17. Here it becomes apparent the benefits that the expansion treatment provides for a specimen even in the presence of a crack. This benefit comes via the reduction of the growth rate while in the compressive region. The importance of the residual compressive stresses in the tangential direction created by the expansion treatment is reiterated in Fig. 17. The compressive stress region counteracts the tensile loading, lessening the effects and the ability for the crack to grow. Recalling from Fig. 12, the residual tangential stress region extended to 4.0 mm away from the edge of hole, looking at Fig. 17 the definition of this region holds as the crack growth is significantly diminished inside the 4.0 mm range. However, outside of the 4.0 mm boundary from the hole edge, the crack grows in a similar manner to the crack in the as-drilled specimen. The reason for this is that the residual compressive stresses no longer are counteracting the applied loads meaning the crack grows faster.

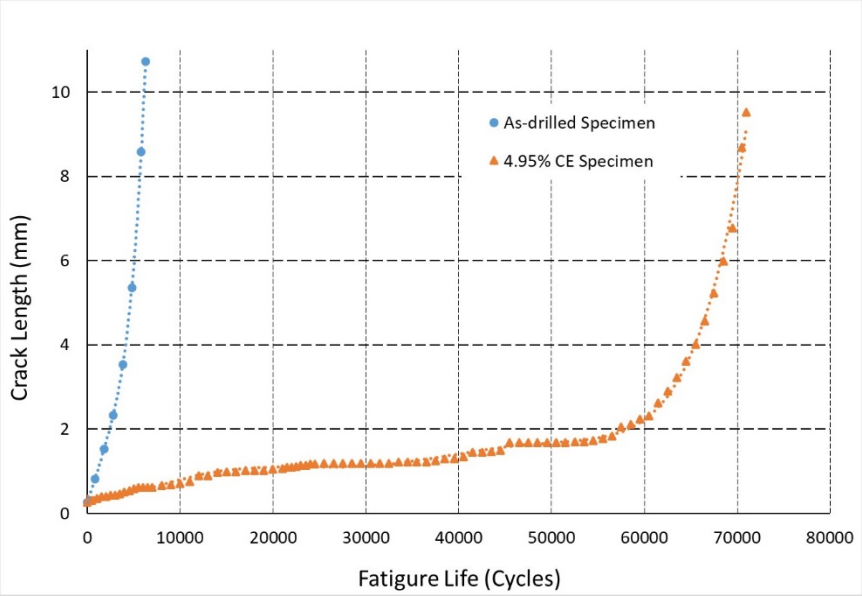

Fig. 17 Crack growth comparison between the as-drilled specimen and cold expanded specimen.

Fatigue Testing in Aggressive Environment

Discovering the benefits that applying expansion treatment to a pre-cracked fastener hole allowed for the examining of the benefits while in the presence of an aggressive environment, in the form of a saline solution. As mentioned previously, three specimens subjected to corrosion were tested. The first experiment was conducted not only to examine the behavior of the fatigue crack in the solution, but also to obtain a fatigue life reference in order to adjust the period of fatigue cycling for future experiments. This first experiment was conducted using the previously mentioned procedures including a 10,000 cycle period between crack growth observations while the specimen was under corrosive environment for 24 hours.

As can be seen in Table 6, this specimen had a final cycle count at failure of 29,433 cycles while undergoing fatigue in a corrosive environment. Figure 18, which is the specimen after failure, shows that the crack grew out across the hole similarly to the two prior fatigue tests. Figure 19 depicts the crack growth during the experimentation. The crack tips are featured by the circles. Variations in lighting assisted in the identification of the crack tip as discontinuities on the metal surface would appear as shadows. It should be noted that in the second image, a sign of corrosion, which is likely the cause of the circular stain around the fastener hole, can be seen on the aluminum surface.

Table 6 Cycle count and crack length for specimen 1 after crack detection and CE treatment.

Cycle Number	Crack Length (mm)
0	0.40
10,356	2.56
20,356	2.66
29,433	9.38

Fig. 18 (a) First specimen just after failure (b) First specimen removed from tensile machine.

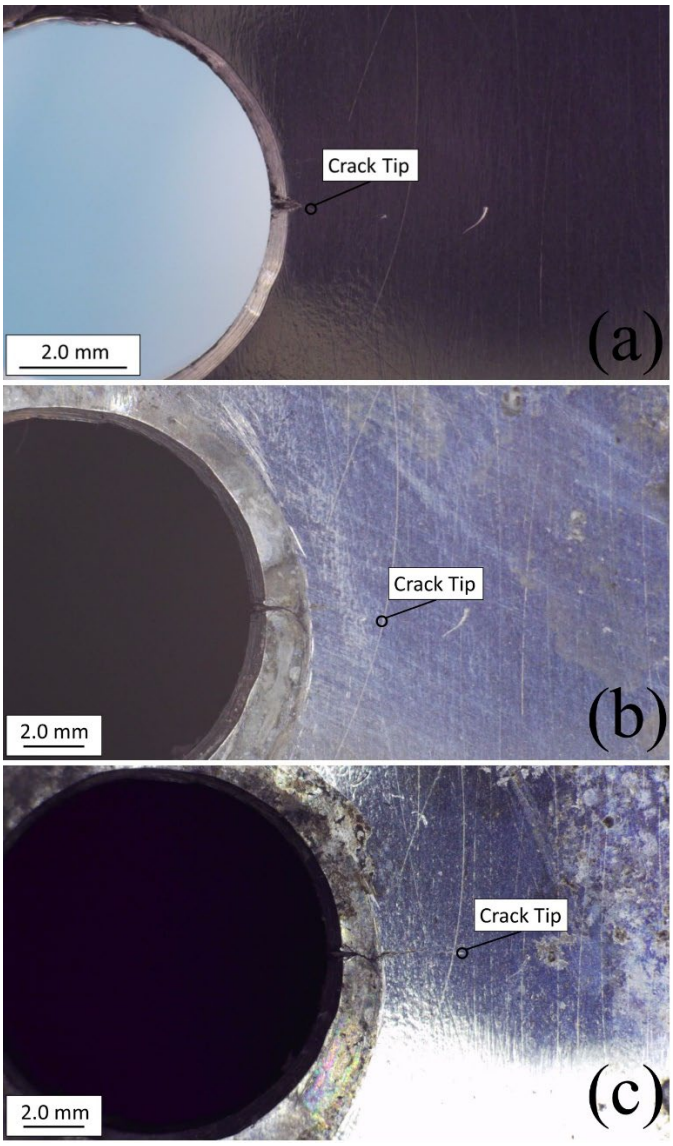

Fig. 19 Crack growth of specimen 1 during fatigue testing (a) 0 cycles (b) 10,356 cycles (c) 20,356 cycles.

Further observations of the images taken during the crack propagation showed salt concentration along the border of the hole and inside the crack, as shown in Fig. 20. This shows that the saline solution is able to seep between the specimen and bolt and be effective as an electrolyte for inducing galvanic corrosion.

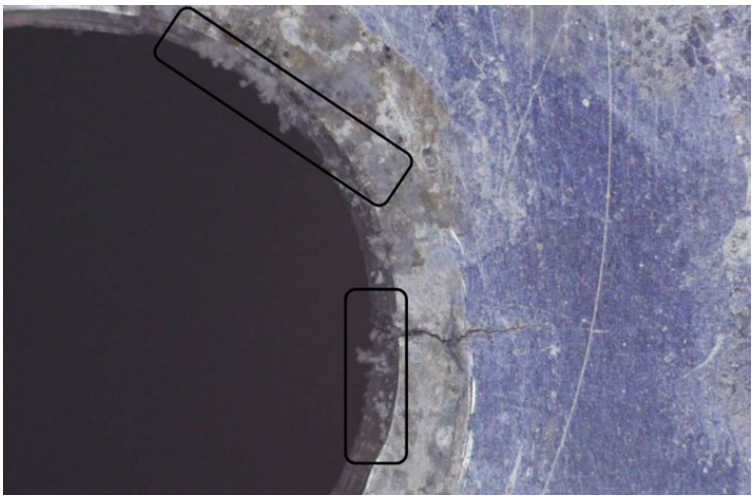

Fig. 20 Close-up image of salt concentration along hole edge.

The fatigue life of this specimen was compared to the previous two experiments, without the corrosive condition, and can be seen in Fig. 21 represented in yellow. The results obtained from this experiment fall in the middle of the lines representing the as-drilled specimen and the cold expanded specimen without the saline solution. The effectiveness of cold work expansion in delaying the crack growth is evident even with the presence of a corrosive environment. However, the effectiveness has also been greatly reduced, as the total fatigue life was less than half of that for the specimen without the saline solution.

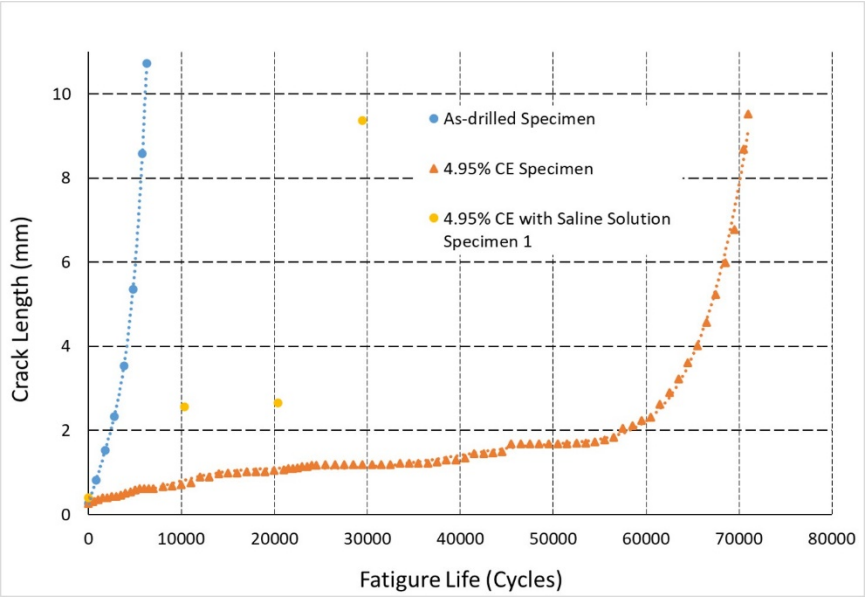

Fig. 21 Crack growth comparison between the as-drilled specimen, cold expanded specimen, and cold expanded specimen with saline solution.

Following the first fatigue testing, the increments for observation was reduced from 10,000 cycles to 3,000 cycles for the second specimen. The change was made to account for an experiment duration of ten days to complete 30,000 total cycles, which was the estimated fatigue life for the specimen under corrosive environment. The number of cycles and the measured crack length during the crack propagation phase (after detection of crack initiation and application of cold expansion treatment) is tabulated in Table 7. It can be seen that specimen 2 withstood a total of 59,413 cycles until ultimate failure, which doubled the fatigue life of 29,433 cycles from the previous specimen.

Table 7 Cycle count and crack length for specimen 2 after crack detection and CE treatment.

Cycle Number	Crack Length (mm)	Cycle Number	Crack Length (mm)
0	0.24	**27,000**	0.83
3,000	0.25	**30,000**	0.87
6,000	0.41	**33,000**	0.88
9,000	0.46	**36,000**	0.88
12,000	0.48	**42,000**	0.88
15,000	0.53	**48,000**	0.88
18,000	0.53	**57,000**	0.94
21,000	0.61	**59,413**	0.94
24,000	0.69		

However, the second fatigue test reached its ultimate failure in a completely different way from specimen 1. Figure 22 shows specimen 2 after failure, as it can be seen the critical crack did not occur from the initial crack at the hole border, but instead, occurred well far from the hole compressive region. Figure 23 provides a closer look at the surface of the crack. It can be seen that the crack initiated from the edge of the specimen on the left of the image and another crack initiation from the right edge as well. These two cracks rather than the crack created at the edge of the hole were what propagated through the specimen leading to failure.

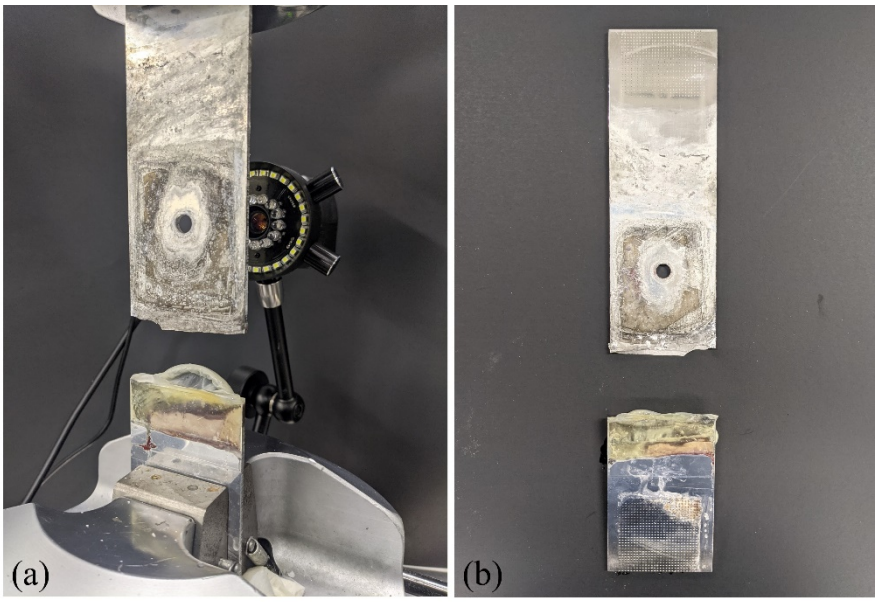

Fig. 22 (a) Specimen 2 just after failure (b) Specimen 2 removed from tensile machine.

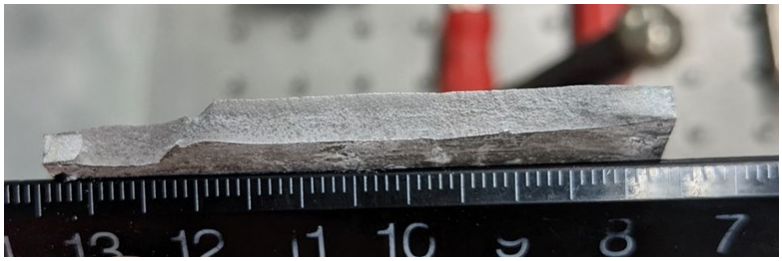

Fig. 23 Close-up image of the crack surface on specimen 2.

Figure 24 shows a closer look at the specimen hole edge at 36,000 cycles. The area featured by the red circle highlights a new crack initiation below the original crack due to local corrosion. Recalling the behavior of crack growth from Table 7, the rate of crack growth was reduced significantly after 33,000 cycles. This occurrence could have been caused by near field parallel cracks interfering in the growth of the original crack. Crack interactions due to multiple cracks can affect the stress intensity factor, crack growth rate, and the crack growth path. A decrease in the stress intensity factor at the crack tips due to the dispersion of tensile stress has been reported for cases when double parallel cracks interacted with each other [21].

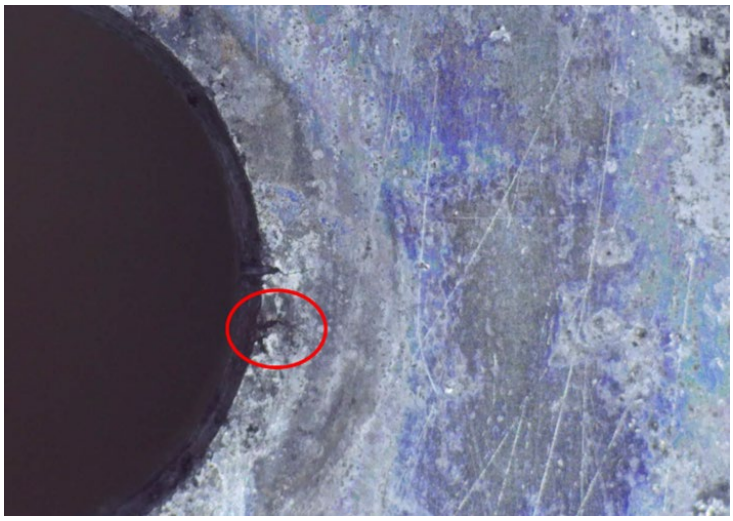

Fig. 24 Close-up image showing a secondary crack parallel to the main crack at 36,000 cycles.

Following the second fatigue testing, another experiment was performed to test if the results from specimen 2 were coincidental or not. The observation increments were reset to be 10,000 cycles. The number of cycles and the measured crack length is summarized in Table 8. As it can be seen, specimen 3 underwent 44,836 cycles before its ultimate failure. Similarly to specimen 2, it failed far from the cold expansion compressive region, as can be seen in Fig. 25. Also similar to specimen 2, upon examining the surface of the crack, Fig. 26, crack initiation can be identified on the right edge of the specimen as well as a very small crack initiation on the left edge.

Table 8 Cycle count and crack length for specimen 3 after crack detection and CE treatment.

Cycle Number	Crack Length (mm)
0	0.32
10,000	0.56
20,000	0.69
30,000	0.75
40,000	0.77
44,836	0.89

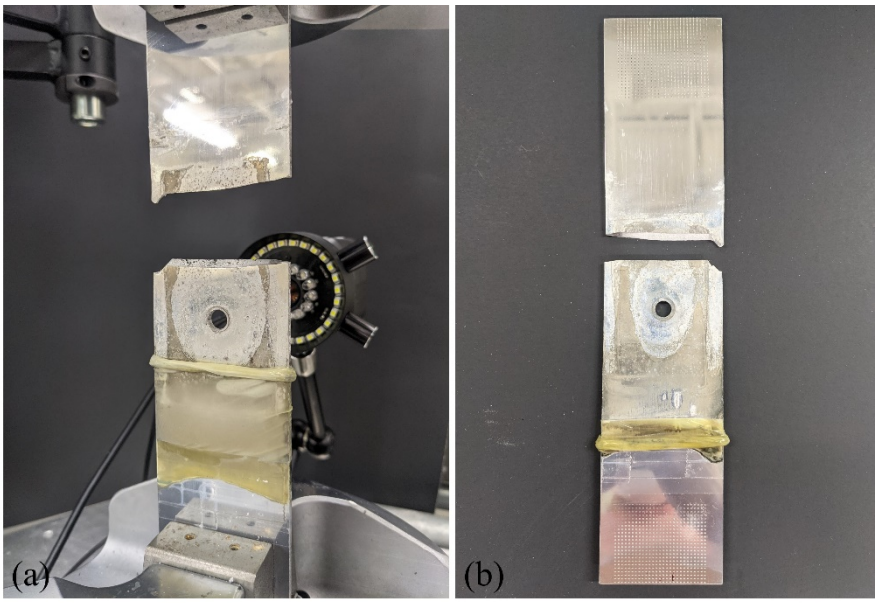

Fig. 25 (a) Specimen 3 just after failure (b) Specimen 3 removed from tensile machine.

Fig. 26 Close-up image of the crack surface on specimen 3.

Finally, the fatigue life of specimen 2 and 3 were added onto the plot comparing the as-drilled specimen, the cold worked specimen without the corrosive condition, and the previous results from specimen 1 in Fig. 27. Data points in green squares and purple diamond markers represent results from specimen 2 and 3 respectively. Results obtained from specimen 2 and 3 follow similar trends to one another. As it can be seen, however, the cracks at the edge of the hole did not reach similar final lengths of other specimens. This is due to the fact that the main cracks that led to failure of these two specimens were not the cracks being monitored. The cracks that did cause failure formed at the edge of the plate, out of the compressive stress region of the cold work expansion.

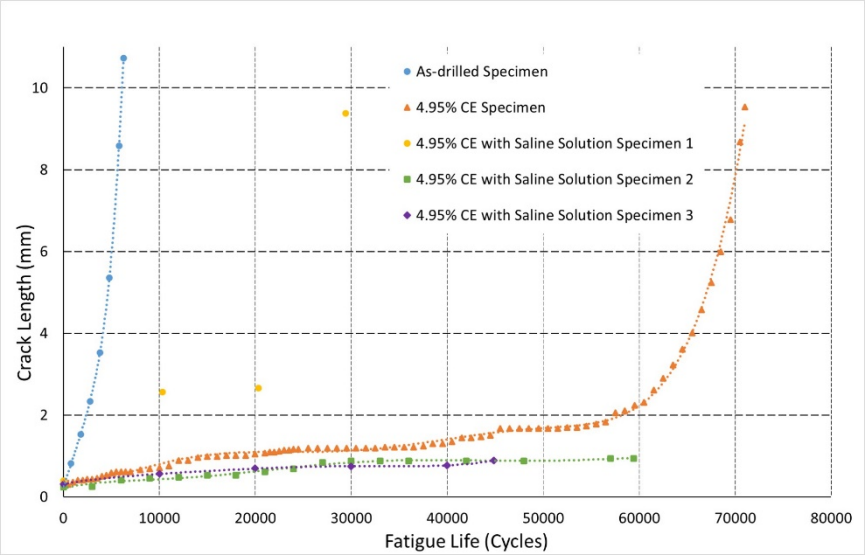

Fig. 27 Crack growth comparison between the as-drilled specimen, cold expanded specimen, and three cold expanded specimens with saline solution.

Numerical Analysis of Specimens in Aggressive Environment

As pointed out in the previous section, crack growth measurements from the second and third fatigue tests do not reflect the growth of the critical crack that led to the ultimate failure of the specimen. Therefore, a numerical analysis utilizing Crack 2000 Damage Tolerance analysis tool [22] was performed to simulate the growth of the critical crack. In addition, the analysis tool was utilized to perform a simulation of a crack propagation of a through crack from a cold expanded hole to compare against results obtained from the first fatigue test. Crack 2000 can correct the stress intensity factor for crack growth simulation of cold worked hole.

In fracture mechanics, stress intensity factor is an important factor to consider, as it is an indicator of the stress state in the vicinity of a crack which helps with making predictions about crack propagation. It is also important to note that stress intensity factor, K, has an additive property meaning that multiple loading conditions can be superimposed, and stress intensity factors can be added based on the condition of interest, as represented in Eq. 11 below presented by Mello [19].

$$K_{eff} = K_{calc} + K_{cold} \tag{11}$$

In the case for a cold expanded hole, for example, the effective stress intensity factor, K_{eff}, is actually the sum of K_{calc}, which is the intensity factor for a plain hole in linear elastic fracture mechanics, and K_{cold}, which is the intensity

factor due to residual stress induced by cold work expansion. As the name implies, the impact is larger as the value K increases. When calculating for K_{cold}, it is known to provide a negative value because of the compressive nature of the residual stress, resulting in a K_{eff} smaller than the plain hole in its "as-is" state. From this perspective, it is known that cold work expansion provides benefits in lowering the impact of stresses as well. For the calculation of K_{cold}, three elements need to be considered. Those are the crack length, hole dimension, and local circumferential stress. While the crack length and hole dimension are either known or can be measured, the local circumferential stress need to be calculated.

Once the local circumferential stress is found, K_{cold} for a two-crack can be found using Green's Function technique in Eq. 12 [19] where c is the crack length, σ_x is the local circumferential stress in the tangential direction calculated by the previous equations, and M_f is the free surface correction based on the ratio of the crack length to the hole radius. This technique integrates the circumferential stresses around the crack, as shown in Fig. 28, to calculate the entire K_{cold}. Shah, who introduced the equation, defined M_f based on the ratio of crack length, c, and radius of the hole, R_h, as depicted by Eq. 13 and Eq. 14 [23].

$$(K_I)_{two\ crack} = \frac{M_f}{\sqrt{\pi c}} \int_{-l}^{l} \sigma_x \left[\frac{c+x}{c-x}\right]^{\frac{1}{2}} dx \tag{12}$$

$$M_f = 1.0 + 0.12\left(\frac{0.3 - \frac{c}{R_h}}{0.3}\right), for\ 0 \leq \frac{c}{R_h} \leq 0.3 \tag{13}$$

$$M_f = 1.0\ , for\ \frac{c}{R_h} > 0.3 \tag{14}$$

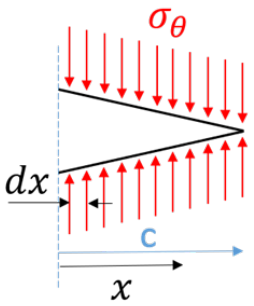

Fig. 28 Variables represented by the Green's Function technique.

As noted before, K_{cold} in the previous equation is actually the stress intensity factor for a two-crack [19]. A two-crack is a situation where two cracks are present in a material, which causes a symmetrical stress loading on the cracks as shown in Fig. 29. In this research, a hole with a single crack is examined making the situation asymmetrical. To take this into account, a conversion shown in Eq. 15 must be performed [19]. Finally, as previously mentioned, this new K_{cold} value is to be added to the "as-is" stress intensity factor to obtain the effective stress intensity factor.

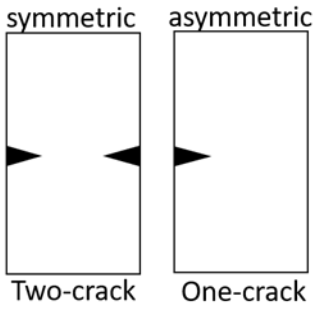

Fig. 29 Comparison of a one-crack and two-crack condition.

$$(K_I)_{one\ crack} = \sqrt{\frac{2R_h + c}{2R_h + 2c}}(K_I)_{two\ crack} \tag{15}$$

For the crack growth simulation, the crack growth model selected for the simulation was the modified Forman equation as explained in [19, 22].

$$\frac{da}{dN} = \frac{C\left[1 - \frac{K_{op}}{K_{max}}\right]^n \Delta K^n \left[1 - \frac{\Delta K_{th}}{\Delta K}\right]^p}{[1-R]^n \left[1 - \frac{\Delta K}{[1-R]K_c}\right]^q} \tag{16}$$

The following values were adopted for the coefficients of the proposed equation as default parameters for AA2024T-3 in the simulation software: $K_{op} = 0.1K_{max}$, $K_{th} = 1.98\ MPa\sqrt{m}$, $n = 4.044$, $p = 0.5$, and $q = 1.0$. In Fig. 30, two new plots are added to the previous results from Fig. 27: the theoretical through crack from the hole and the theoretical corner crack from the edge of a plate. The model chosen for the corner crack was the one defined in the simulation software [19, 22] as "Corner Crack from a hole in a Plate". For this model, the software independently computes the stress intensity factor for the thickness and width fronts, and then assumes the crack growing in an elliptical shape. One hypothesis behind the longer time predicted by crack simulation on the edge of a hole, when

compared with the experimental result, is that for the first measurement the crack length was not totally visible and the crack could be much larger on the back of the plate (1-2 mm), causing a jump between the first and second measurements. The time frame between second, third and fourth measurements follow the time frame in the simulation. It should be noted that the material property used for these plots were AA2024-T351 alloy under corrosive environment of 3.5 wt.% NaCl solution, as it was the closest material to AA2024-T3 alloy among other materials accommodating for corrosion available in the software. However, the properties are similar enough for sufficient qualitative comparison. Some material properties used in the software are presented in Table 9.

When comparing the two theoretical curves, it can be seen that the through crack from the hole will result in a shorter fatigue life compared to the corner crack at the edge of the plate. In addition, for both theoretical curves, a decrease in total fatigue life compared to the cold expanded specimen without the saline solution can be seen. This is because the material properties of the material declined due to the corrosive condition.

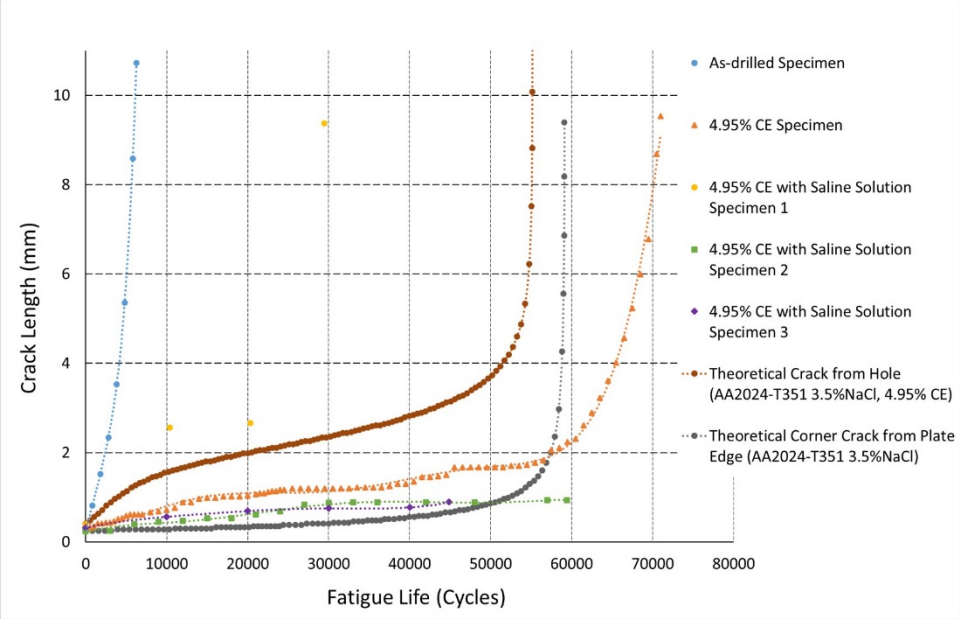

Fig. 30 Crack growth comparison between experimental results and theoretical simulation of a through crack from a hole and a corner crack from the plate edge of an AA2024-T351 alloy under corrosive condition.

Table 9 Material properties of AA2024-T351 alloy under influence of 3.5 wt.% NaCl solution [19].

Property	Value
Yield Strength	345 MPa
Ultimate Strength	427 MPa
Effective fracture toughness, K_{i_e}	48.0
Plane strain fracture toughness, K_{i_c}	34.0
Plane stress fracture toughness, K_c	67.6

The theoretical curve for the corner crack from the edge of a plate in Fig. 30 was simulated for an initial crack length and depth of 0.25 mm. This value was found by an iterative process to find an initial crack length that would yield a total fatigue life of approximately 59,413 cycles seen from specimen 2. Results from the simulation indicated that the crack tolerates 59,117 cycles until failure at critical crack length of 9.40. This simulation implies that for the material to fail as it did for specimen 2, an initial crack length of 0.25 mm must be present early on during the crack propagation process. It is likely that cathodic particles near the edge of the specimen corroded the base material to cause a pit formation, as described by Nicolas et al. [14], causing the new crack formation and a propagation of the secondary crack to move more rapidly than the original crack in the expanded hole.

On the other hand, the theoretical curve for the through crack at the hole indicates a significant difference compared with the specimen 1 results. The curve illustrates a total fatigue life of 55,169 cycles and a critical crack length of 15.54 mm. The actual life was 53% of that, failing at only 29,433 cycles.

Combining the results from the comparison, it is likely that the simulations do not represent the entire picture, as it does not take in to account the formation of multiple cracks due to the effect of corrosion. Associated with that, it is known that AA2024-T351 used in the analysis has a slightly better fatigue and corrosion resistance than the AA2024-T3 used in the experiment. Despite having exactly the same chemical composition, both being solution heat-treated, stress relieved, then naturally aged, what would indicate similar distribution of cathodic precipitates [13, 14], simulations with the mechanical properties in laboratory environment of both materials show a 5 to 10% difference in crack propagation rate between the two materials.

V. Discussion

A. Remarks

- After conducting analytical calculations using Elastic-Plastic Theory Equations, the residual effects caused by the expansion application could be analyzed. It was found that residual stresses in the tangential direction have the most important impact on fatigue life benefits. These high compressive stress values that make up the tangential stress region would counteract the tensile loading applied to the specimen. For the specimen dimensions and boundary conditions used in this research, it was determined that the compressive stress region would retard crack growth in the region up to 4.0 mm away from the hole edge.
- Fatiguing specimens revealed the benefits that cold hole expansion can provide even when there is a presence of pre-cracks. It shows that cold work can be applied in the field to in use structures, even with limitation of damaged material removal, reaming and finishing of fastener holes. The specimen that did not receive any cold expansion after the detection of a small crack was able to withstand 6,356 cycles of high loading stresses. The specimen that did receive expansion after the small crack was detected was able to withstand 70,983 cycles at the same loading parameters.
- The specimen that underwent cold expansion had a fatigue life improvement of 11.3 times that of the as-drilled specimen. This is a significant improvement on fatigue life even though there was a crack present at the time of application. The effect of the compressive stress region developed by the expansion could be seen as well as noted by the minute changes in crack length as seen in Fig. 17. The compressive stress region was determined to slow down the crack growth by counteracting the tensile loading applied during the fatigue testing.
- Upon conducting the first fatigue testing, the fatigue life of the cold expanded and saline solution exposed AA2024-T3 sample showed a decrease compared to the cold expanded specimen without the corrosive solution. However, the fatigue life continued to be larger than that of the specimen without the cold expansion treatment by over 4 times. It was determined that the effect of cold work expansion in delaying crack growth remains even with the presence of a corrosive condition. No secondary crack was observed during this experiment.
- Following the second fatigue under corrosion testing, ultimate failure was found not at the pre-cracked hole, but significantly far from the hole edge outside of the compressive stress region induced by the cold work expansion. The third fatigue testing demonstrated similar results as the second fatigue testing in that the location of

the ultimate failure was, again, found out of the compressive zone caused by the cold expansion. Examination of the fracture from both second and third fatigue testing exhibited signs of a shift in the fatigue critical location.

- The specimen benefited from cold work expansion, as demonstrated in previous works, in reducing the stress intensity factor of the initial crack. However, the corrosion exposure created a new site away from the compressive region where the new crack initiated and became the critical path to failure. Additionally, parallel cracks caused by corrosion formed around the hole border due to local corrosion causing a reduction of stress intensity factor at the original crack, a decrease in crack growth rate, making the new crack away from the original crack, the most critical for the specimen.
- Under corrosion we have seen that the fatigue critical location of the tested specimen with a cold worked hole migrated from the hole to the edge of the plate, out of the compressive region as the location of the critical stress intensity factor moved. At the edge of the plate, corrosion may induce rapid crack initiation due to pitting formation.
- It is clear that the effect of the galvanic corrosion was not only at the vicinity of the cathode, but was expanded for all the region subjected to the corrosive environment. The secondary cracks for specimens 2 and 3 formed more than 20 mm away from the cathodic Type AISI 316 stainless steel bolt.
- Lap joints with cold worked holes and connected by dissimilar material fasteners, which have been previously analyzed for crack propagation under corrosive environment, must be reanalyzed considering an additional edge crack out of the compressive zone of the structural joint. The inspection intervals must also be reevaluated based on the most critical crack propagation rate under presence of aggressive environment.

B. Recommendations

- The applied stress during the fatigue cycles was rather high to ensure the specimens in this experiment would present crack propagation within a reasonable time. This implied that the stresses applied were able to overcome the compressive stress regions developed by the cold expansion as the crack grew. One avenue of future research would be to examine the full effect that the current level of applied cold expansion would have if the applied stresses were lower.
- Comprehensive monitoring of the area under corrosion is recommended to not only follow the path of the main crack, but to expand the view for potential critical cracks forming far from the hole. Data of the crack leading to the ultimate failure will provide a better fitting curve and material properties for the specific environment. For the

same purpose of investigation, another approach is to keep the corrosion confined to the hole region to better control and follow the main crack growth or initiation nearby.

- Local investigation of the initiation site with Scanning Electron Microscope (SEM) is also recommended. This research places emphasis on the effects of cold expansion and the resulting residual stress on the crack growth in a corrosive environment. As seen from the theoretical curves, corrosion has shown significant effects on the crack growth. Therefore, the electrochemistry aspect of the material should be examined along with the microstructure of the material. As the new crack starts, the specimen can be removed and observed under SEM in order to identify the cause of the new crack initiation. As observed by Nicolas et al. the probable cause could be a local corrosion around a cathodic precipitate [14].
- The fractured specimen can be cut and prepared in order to observe the crack surface under SEM. With this, identifying the local pit formation at the plate edge, the point of crack initiation, the initial crack size, and the propagation path for specimen 2 and 3 will be possible. Using striation counting technique, we can estimate the number of cycles to failure and, consequently, the time necessary for the crack initiation under aggressive environment.

VI. Conclusion

The application of cold work hole expansion to fastener holes in AA 2024-T3 was found to provide benefits to the overall fatigue life even with cracks present at the hole and in an aggressive environment. Cold hole expansion created residual compressive stresses around fastener holes that slowed the crack growth rate, thus providing fatigue life benefits, such as an improved inspection interval, to the overall structure. The research also displayed signs of a location shift in critical stress intensity factor due to the corrosive environment, which an evaluation of the inspection area may be necessary in future research for the prevention of a secondary crack initiation.

References

[1] Mostefa, B., Abdelkrim, A., Ali, B., and Mohamed, B., “Effect of hardening induced by cold expansion on damage fatigue accumulation and life assessment of Aluminum alloy 6082 T6,” Materials Research, vol. 15, 2012, pp. 981–985. doi: https://doi.org/10.1590/S1516-14392012005000123

[2] Wang, Y., Zhu, Y., Hou, S., Sun, H., and Zhou, Y., “Investigation on fatigue performance of cold expansion holes of 6061-T6 aluminum alloy,” International Journal of Fatigue, vol. 95, 2017, pp. 216–228. doi: https://doi.org/10.1016/j.ijfatigue.2016.10.030

[3] Liu, J., Shao, X. J., Liu, Y. S., and Yue, Z. F., “Effect of cold expansion on fatigue performance of open holes,” Materials Science and Engineering: A, vol. 477, 2008, pp. 271–276.
doi: https://doi.org/10.1016/j.msea.2007.05.034

[4] Pasta, S., “Fatigue crack propagation from a cold-worked hole,” Engineering Fracture Mechanics, vol. 74, 2007, pp. 1525–1538.
doi: https://doi.org/10.1016/j.engfracmech.2006.08.006

[5] Gopalakrishna, H. D., Narasimha Murthy, H. N., Krishna, M., Vinod, M. S., and Suresh, A. V., “Cold expansion of holes and resulting fatigue life enhancement and residual stresses in Al 2024 T3 alloy – An experimental study,” Engineering Failure Analysis, vol. 17, 2010, pp. 361–368.
doi: https://doi.org/10.1016/j.engfailanal.2009.08.002

[6] Citarella, R., Cricri, G., Lepore, M. A., Perrella, M. “Assessment of Crack Growth from a Cold Worked Hole by Coupled FEM-DBEM Approach”, Key Engineering Materials. 577-578. 669-672, 2013.
doi: https://doi.org/10.4028/www.scientific.net/KEM.577-578.669

[7] Phillips, J. L., “Sleeve coldworking of fastener holes,” Ohio: Wright-Patterson Air Force Base, 1974

[8] Chakherlou, T. N., and Vogwell, J., “The effect of cold expansion on improving the fatigue life of fastener holes,” Engineering Failure Analysis, vol. 10, 2003, pp. 13–24.
doi: https://doi.org/10.1016/S1350-6307(02)00028-6

[9] Zhang, X., and Wang, Z., “Fatigue life improvement in fatigue-aged fastener holes using the cold expansion technique,” International Journal of Fatigue, vol. 25, 2003, pp. 1249–1257.
doi: https://doi.org/10.1016/S0142-1123(03)00152-X

[10] Snihirova, D., Höche, D., Lamaka, S., Mir, Z., Hack, T., and Zheludkevich, M. L., “Galvanic corrosion of Ti6Al4V - AA2024 joints in aircraft environment: Modelling and experimental validation,” Corrosion Science, vol. 157, 2019, pp. 70–78.
doi: https://doi.org/10.1016/j.corsci.2019.04.036

[11] Czaban, M., “Aircraft Corrosion – Review of Corrosion Processes and its Effects in Selected Cases,” Fatigue of Aircraft Structures, vol. 2018, 2018, pp. 5–20.
doi: https://doi.org/10.2478/fas-2018-0001

[12] NACE International, “Galvanic Corrosion,” AMPP Available: https://www.nace.org/resources/general-resources/corrosion-basics/group-1/galvanic-corrosion.

[13] Nicolas, A., Mello, A. W., and Sangid, M. D., “The Effect of Strain Localization on Galvanic Corrosion Pitting in AA7050,” Corrosion, vol. 74, 2018, pp. 860–872.

doi: https://doi.org/10.5006/2729

[14] Nicolas, A., Mello, A. W., and Sangid, M. D., "Relationships between microstructure and micromechanical stresses on local pitting during galvanic corrosion in AA7050," Corrosion Science, vol. 154, 2019, pp. 208–225.
doi: https://doi.org/10.1016/j.corsci.2019.03.016

[15] Mello, A. W., Nicolas, A., Lebensohn, R. A., and Sangid, M. D., "Effect of microstructure on strain localization in a 7050 aluminum alloy: Comparison of experiments and modeling for various textures," Materials Science and Engineering: A, vol. 661, 2016, pp. 187–197.
doi: https://doi.org/10.1016/j.msea.2016.03.012

[16] Dowling, N. E., Mechanical behavior of materials: engineering methods for deformation, fracture, and fatigue, Englewood Cliffs, NJ: Prentice-Hall, 2012.

[17] DOD, Military handbook: metallic materials and elements for aerospace vehicle structures, United States Department of Defense, 2003.

[18] Cardinal, J. W., Wieland, D. H., Cutshall, J. T., and Burnside, H. O., "Analysis of cold worked holes for structural life extension," Sep. 1994.

[19] Mello, A. W. S., "CRACK 2000 Program User's Manual (2.1 ed.) ," 1998.

[20] Rice, R. C., Jackson, J. L., Bakuckas, J., and Thompson, S. (n.d.). "Metallic Materials Properties". Development and Standardization *(MMPDS)* (Rep. No. DOT/FAA/AR-MMPDS-01). Washington D.C.: U.S. Department of Transportation - Federal Aviation Administration - Office of Aviation Research.

[21] Han, Z., Qian, C., and Li, H., "Investigation of the Enhancement Interactions between Double Parallel Cracks on Fatigue Growth Behaviors," Materials, vol. 13, 2020, p. 2952.
doi: https://doi.org/10.3390/ma13132952

[22] Mello, A. W. S., "CRACK 2000," 2005.

[23] Rooke, D. P., Baratta, F. I., and Cartwright, D. J., "Simple methods of determining stress intensity factors," Engineering Fracture Mechanics, vol. 14, 1981, pp. 397–426.
doi: https://doi.org/10.1016/0013-7944(81)90010-2